United States Environmental Protection Agency

EPA/600/S-17/256 | October 2017 | www.epa.gov/research

Description of Changes in Climatic Indices in USA over 25 Years (1989 – 2013)

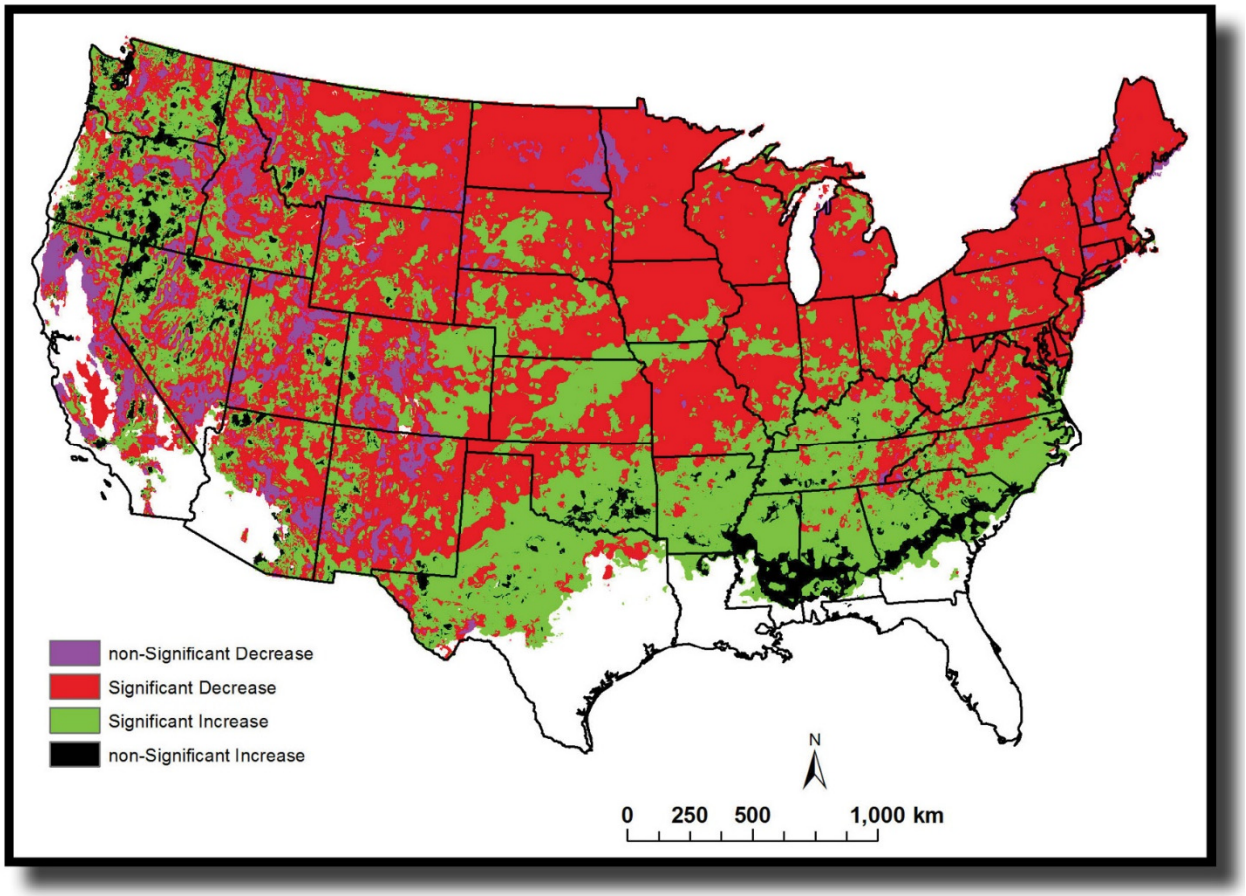

Trend of annual number of months with at least one month that had a day with a minimum temperature < 0°C over 25 years

RESEARCH AND DEVELOPMENT

Description of Changes in Climatic Indices in USA over 25 Years (1989 – 2013)

Prepared by

Maliha S. Nash[1], Jay R. Christensen[2]

[1]U.S. Environmental Protection Agency, Office of Research and Development,
Ecological & Human Community Analysis Branch, Las Vegas, Nevada, USA

[2]U.S. Environmental Protection Agency, Office of Research and Development,
Ecosystem Integrity Branch,
Las Vegas, Nevada, USA

U.S. Environmental Protection Agency
Office of Research and Development
Washington, DC 20460

Acknowledgements

We are grateful for the valuable inputs and suggestions provided by Drs. Mike McDonald, James Wickham, and Taylor Jarnagin which improved the comprehensiveness and clarity of this report.

Notice

The U.S. Environmental Protection Agency (EPA), through its Office of Research and Development (ORD), funded and performed the research described here. It has been peer-reviewed by the EPA and approved for publication, but it may not necessarily reflect official Agency policy. Mention of trade names or commercial products does not constitute endorsement or recommendation for use.

Table of Contents

List of Figures

List of Figures (cont.)

List of Figures (cont.)

Acronyms and Abbreviations

AT	Apparent Heat
CV	Coefficient of Variability (standard deviation/mean)
DP	Dew Point Temperature
FEM	Freshwater Ecosystem Mosaic
MI	Moisture Index
NDVI	Normalized Difference Vegetation Index
PET	Potential Evapotranspiration
PRISM	Parameter-Elevation Regressions on Independent Slopes Model
RF	Rainfall

Introduction

The spatial distribution of long-term changes in climatic factors and its relation with vegetation cover, human health, hydrology and many other ecosystem processes help to identify the consequences of climatic factors changes. In recent studies, the significant changes of selected climatic factors over 25 years has been associated with changes in greenness (Nash et al. 2017), with shifts in health outcomes (Perry et al. 2011), and with fog formation (Hiatt et al. 2012) as examples of the impacts of climate factors on ecosystems and societal benefits. This report concentrates on the methodology and potential future uses for long-term climate factor trends, and trends of derived climatic factors and indices. Analyses of all factors over the 25 years (1989-2013) show the magnitude and direction of significant changes on different time scales (monthly, annual average, and seasonal). Additionally, annual averages, coefficient of variation (CV), first and 99th percentile were also presented to show the differences in patterns of variability and extreme values. The climate factors considered are: Minimum, maximum and dew temperatures, and precipitation. A derived climatic factor considered was: potential evapotranspiration (PET); and two climatic indices were a moisture index and an apparent temperatures (*AT*) index, or Heat Index (Smoyer-Tomic and Rainham 2001). All of our analyses were performed per 1 km^2 pixels for the contiguous U.S. and we present the spatial distribution of temporal changes of:

1- the significant ***monthly*** changes in climatic information over 25 years via maps and a statistical summary description of results (n=300),
2- the significant ***annual*** changes in climatic information via maps and a statistical summary description of results (n=25),
3- significant ***seasonal*** changes for precipitation, PET, and MI via maps and a statistical summary description of results (n=25),

4- comparison of the spatial distribution patterns of 1-3, and

5- distribution of heat index (*AT*) groups as it relates to health consequences.

These long-term datasets and trends in temperature and precipitation can be used to study (among other things) the influence of precipitation and temperature trends on potential shifts in water storage, hydrological flows, biogeochemical processes or biological shifts on water-dependent species. Two studies have already begun to utilize the summarization of the 25-year climate and derivative datasets. A drought resilience study led by EPA NCEA and USGS has included the 25-year summaries of climate variables to help explain changes in water storage as measured by inundation maps (Vanderhoof et al. in prep). In another study, the climate variables are being combined with waterbody data and landscape features to describe the collection of aquatic habitats for biological species and their patterns of occurrence within a matrix as a "freshwater ecosystem mosaic" (FEM). Our intent was to make the methodology, data, and analyses available for research efforts such as these, to better understand the trends of precipitation, temperature, and their interactions in hydrological, societal, biological and ecological systems.

Method and Materials

Monthly averages of precipitation, maximum temperature, minimum temperature, and dew point temperature were obtained from Parameter-elevation Regressions on Independent Slopes Model (PRISM; http://www.prism.oregonstate.edu/products/matrix.phtml, accessed October 2017). PRISM climatic factors from 1989-2013 at a resolution of 4-km^2 grid cell were gridded into 1-km^2 grid cells using the inverse distance weighted method in ARC-GIS 9.3.1 (ESRI, Redlands, California) to match the NDVI resolution (Nash et al. 2017). Downscaling of PRISM climate data from 4 km^2 to 1 km^2 was also applied by Thorne et al. (2012).

Potential Evapotranspiration

We derived PET following Hamon (1961) and Enquist et al. (2008) as:

$$PET = 13.97\, dD^2 W_t \qquad [1]$$

$$W_t = 0.0495 e^{0.062T} \qquad [2]$$

where d is number of days in a month, D is mean monthly hours of daylight (in unit of 12 hours), W_t is saturated water vapor density and T is the monthly mean temperature in ºC. PET is in units of mm/month. The mean day length (D) was calculated as:

$$D = 24 - \frac{24}{\pi}\, Arcsin\left[\frac{sin\frac{\rho\pi}{180} + sin\,\frac{L\pi}{180} sin\varphi}{cos\frac{L\pi}{180} cos\varphi}\right]$$

$$\theta = 0.2163108 + 2 * Arctan\,\{0.9617396 * Tan\,[0.0086*(J\text{-}186)]\}$$

$$\varphi = Arcsine(0.39795 * cos\theta)$$

where θ is revolution angle (radians), φ is sun's declination angle (radians), p is daylight coefficient (degrees) (=0.8333; Forsythe et al. 1995), L is latitude, and D is daylight length.

Moisture Index

The moisture index (MI), also known as climatic moisture index (Willmott and Feddema, 1992), combines rainfall (RF) and PET as:

$$MI = \begin{cases} \frac{RF}{PET} - 1 & if\ RF < PET \\ 1 - \frac{PET}{RF} & if\ RF \geq PET \\ 0 & if\ PET = RF = 0 \end{cases} \quad [3]$$

MI value ranged from -1 to +1 representing the relative moisture in the environment from driest to wettest moisture conditions. For annual and seasonal MI, summation of PET and RF for the year and season were used. Seasons were winter (December, January, February), spring (March, April, May), summer (June, July, August) and fall (September, October, November). Feddema (2005) grouped the MI into six moisture regimes: very wet [MI ≥ 0.66], wet [0.66 > MI ≥ 0.33], moist [0.33 > MI ≥ 0.00], dry [0.00 > MI ≥ -0.33], semi-arid [-0.33 > MI ≥ -0.66]; and arid [MI < -0.66]; we also used the same groups, but added a zero group as a divider between dry and wet areas (see map in Fig. 6B).

Apparent Heat

Apparent heat (*AT*), derived by Smoyer-Tomic and Rainham (2001) (also known as the index of heat (Perry et al. 2011)) combines daily temperature and humidity as:

$$AT = -2.719 + 0.944 * T + 0.016 * DP^2 \quad [4]$$

where *AT* is apparent temperature, *T* is the air average temperature (°C) and *DP* is the dew point temperature (°C). Smoyer-Tomic and Rainham (2001) used *AT* to monitor heat waves and grouped *AT* into four health impact related classes related to fatigue, two levels of sunstroke, and heatstroke. Although *AT* was developed as a daily heat index, our analyses were done monthly to show the

spatial distribution of the number of months with at least one event in Smoyer-Tomic and Rainham (2001) groups. These four *AT* groups are described below:

a) *fatigue possible with prolonged exposure and/or physical activity* (26.7°C ≤ *TA* ≤ 32.2°C)
b) *sunstroke, heat cramp, and heat exhaustion possible with prolonged exposure and/or physical activity* (32.2°C < *AT* ≤ 40.6°C)
c) *sunstroke, heat cramp, or heat exhaustion likely, and heatstroke possible with prolonged exposure and/or physical activity* (40.6°C < *AT* ≤ 54.4°C)
d) *heatstroke/sunstroke highly likely with continued exposure* (*AT* > 54.4°C).

The spatial distribution of the significance and direction of the *AT* trends were also presented.

Annual and seasonal averages of precipitation (with coefficients of variation) were derived for 25 years (n=25). The four seasons are: Winter (December – February), spring (March – May), summer (June – August) and fall (September – November). Averages and coefficients of variation for annual precipitation and PET were also determined. Changes in minimum temperature were described by equating number of months per year with at least one Day of < 0°C. The trend in the number of months per year with minimum temperature < 0°C was determined over the USA. The direction and significance level of the trend were presented in a map view to show the spatial locations of changes. We also present the 1st and 99th percentiles to spatially locate the extremes.

Univariate Autoregression

We used univariate autoregression to quantify the temporal trend (slope) for each of the climate factors and derived variables to identify the general pattern of change for each variable over the 25-year period. The trend values, direction, and probability of each pixel was then mapped to identify geographic patterns of the trend direction. Time series regression

(autoregression) was used in both analyses because errors in temporal data may be dependent (e.g., consecutive times, annual cycles). If dependency exists and is not corrected, then the standard error of the estimate (e.g., slope) would be inflated, and the significance level for the slope and other estimates would be incorrect. Below we detail the analyses.

Trends in the individual climate factors over the 25-year period were addressed for each 1-km^2 pixel by using an autoregression model (Proc Autoreg; SAS/ETS, 1999) with stepwise selection. Significant autoregressive error was fit to the observed values to define the direction and p-value for the slope, where:

$$Y_t = \theta_o + \theta_1 * Time + \mu_t \qquad [5]$$
$$\mu_t = \sum_{t=1}^{k} \rho_i \mu_{t-i} + \varepsilon_t$$
$$\varepsilon_t \sim IN(0, \sigma^2)$$

where Y is an individual time series variable (e.g., monthly precipitation, maximum temperature, minimum temperature, monthly dew point temperature, and MI (n=300 months)). The fitted autoregression model for the observed variable (Y_t) is the same as that of an ordinary least square regression model (OLS; $\theta_o + \theta_1 * Time$), plus the autoregressive error (u_t). Coefficients θ_o, and θ_1 are the intercept and the slope with time, respectively. The time series error term, u_t, may be autocorrelated. The term $\sum_{i}^{k} \rho_i u_{t-i}$ is the summation of the significant autoregressive parameter (ρ) times lagged time series error(s), and k is the order of significant lags in the model. The error term, ε_t, from the autoregressive error model is normally and independently distributed (*IN*) with a mean of zero and variance σ^2. The slope (θ_1) quantifies the rate and direction of change for each variable over 25 years in each 1 km^2 pixel. A significance level of $p < 0.05$ was used to test whether the slope differed from zero.

Results

Monthly: Minimum Temperature, Maximum Temperature, Dew Point Temperature, Precipitation, Potential Evapotranspiration (PET), Moisture Index (MI), and Apparent Heat (AT).

Significant maximum and minimum temperature increases covered 12% and 35% of the contiguous United States, respectively (inset maps in Fig. 1) (Nash et al. 2017). Significant increases in maximum temperature (inset map in Fig. 1A) were concentrated in New England, Texas, and Louisiana, but also scattered throughout the western United States. The spatial distribution of maximum temperature trend values (Fig. 1A) shows that the 1st and the 99th percentiles of the trend values were + 0.0067°C/month and -0.0069°C/month, respectively. The clusters of increasing maximum temperature are situated on a diagonal path from Texas to Washington, with additional clusters in the state of California situated mostly in Stanislaus, Inyo, and Sequoia national forests. North Dakota, the eastern side of Montana, and the Pacific coast of Oregon and Washington had a decreasing trend in maximum temperature. The decrease in North Dakota and eastern side of Montana was not significant (inset map in Fig. 1A).

Significant minimum temperature (Fig. 1B) increases were common throughout the contiguous United States, except for the upper Midwest. The 1st and the 99th percentiles of the trend values were -0.0064°C/month and +0.0144°C/month for the minimum temperature (Fig. 1B). The clusters of trend values showed a mosaic pattern in the western states, in contrast to the mid and eastern states where the clusters are larger in size. This pattern of clustering indicates that higher variability in minimum temperatures may occur where extremes in higher and lower nighttime temperatures are more apparent (e.g., in the western U.S. relative to the eastern U.S.). Most of Oregon and Washington experienced a decrease in minimum temperature, while California was more of a mosaic. In California, the minimum temperature mostly increased in the

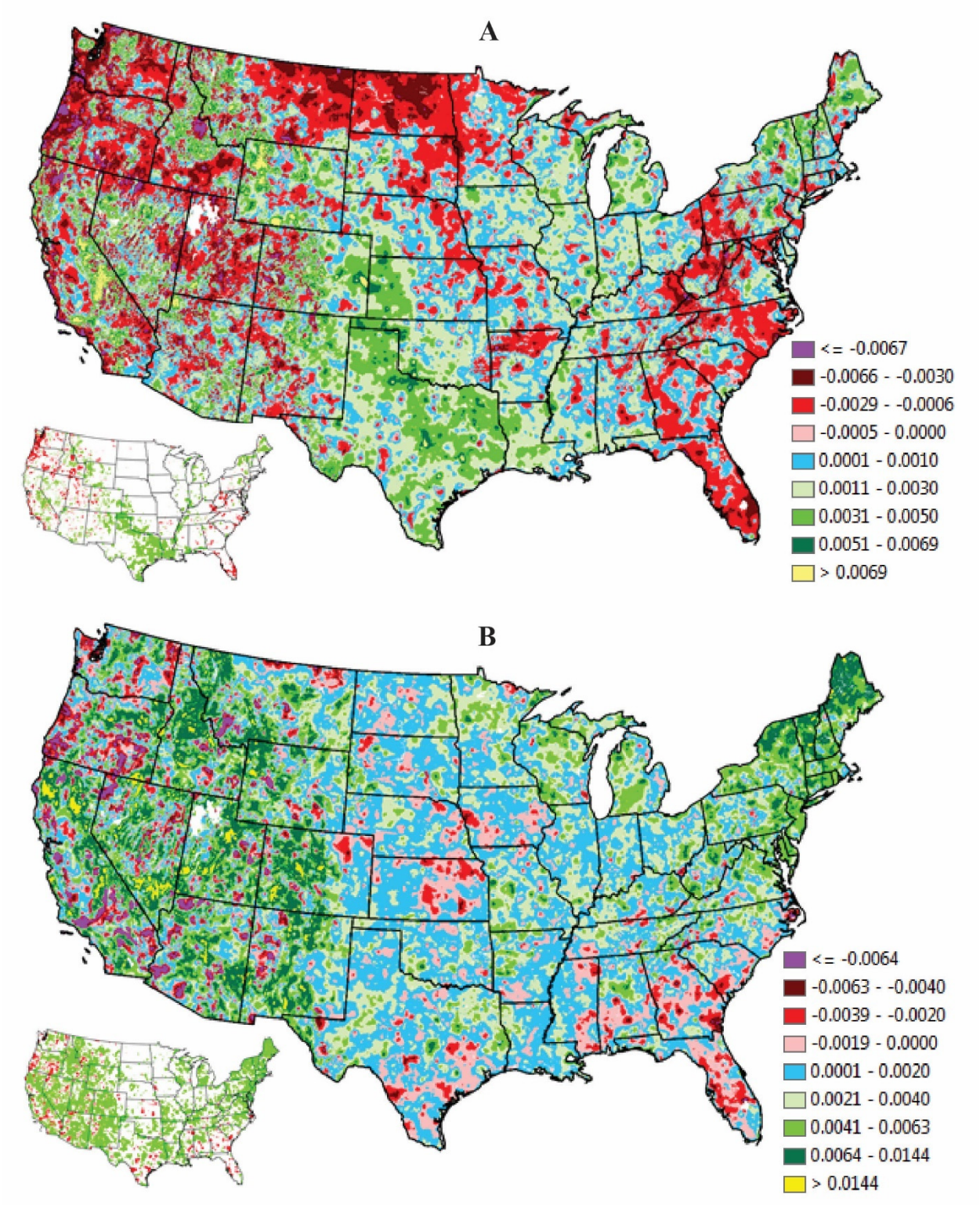

Figure 1. Pixels (1 km^2) with temporal trends in monthly (A) maximum temperature and (B) minimum temperature (°C/month). The first and last legend classes represent the 1st and 99th percentiles. The insets are the probability of temporal trend, green indicates significant increase; red indicates significant decrease.

mountainous national forest areas (e.g. Shasta, Trinity, Six Rivers, Lassen, Plumas, Tahoe, Humboldt, and Los Padres National Forests.) The increasing minimum temperatures over the 25 years in Wyoming, Colorado, and New Mexico coincide with tree mortality and wildfire (Nash et al. 2014, 2017). In the east, the greatest increase in minimum temperature was in north Maine, Vermont, New York (Fig. 1B) and to a lesser level in Pennsylvania to eastern North Carolina.

The significant decrease in both minimum and maximum temperatures covered an approximately similar percentage of area (~4%), but were more "patchy." Areas of significant minimum and maximum temperature decreases were scattered throughout the contiguous United States, but predominately in the south and the west. The general trend over the last 25 years has been for monthly minimum temperature to increase significantly for a substantial proportion of the continental U.S. (inset map in Fig. 1B). The annual number of months with < 0°C is decreasing as well. The trend of annual number of months with at least one month that had a day with a minimum temperature of < 0°C decreased in 49.9% of the U.S. (Fig. 2) and significantly increased in 23.9% of the U.S. The number of months with minimum temperature < 0°C did not change significantly over the 25 years in 26.2% of the U.S. and were mostly in the southern U.S. The number of cold months increased primarily in eastern-southern part of the U.S. and in a mosaic pattern in Washington, Oregon, Nevada. The number of months with freezing conditions decreased in the Northern U.S, especially within the Northern Great Plains and in the Northeastern states. Significant increases in months with freezing conditions were found in a band from Texas to North Carolina (Fig.2).

Significant dew point temperature changes were regionally diverse (Fig. 3), exhibiting significant increases in the east and significant decreases in the west. The contiguous clusters of pixels (red pixels in the map inset in Fig. 3) with a decrease in dew point temperature were mainly

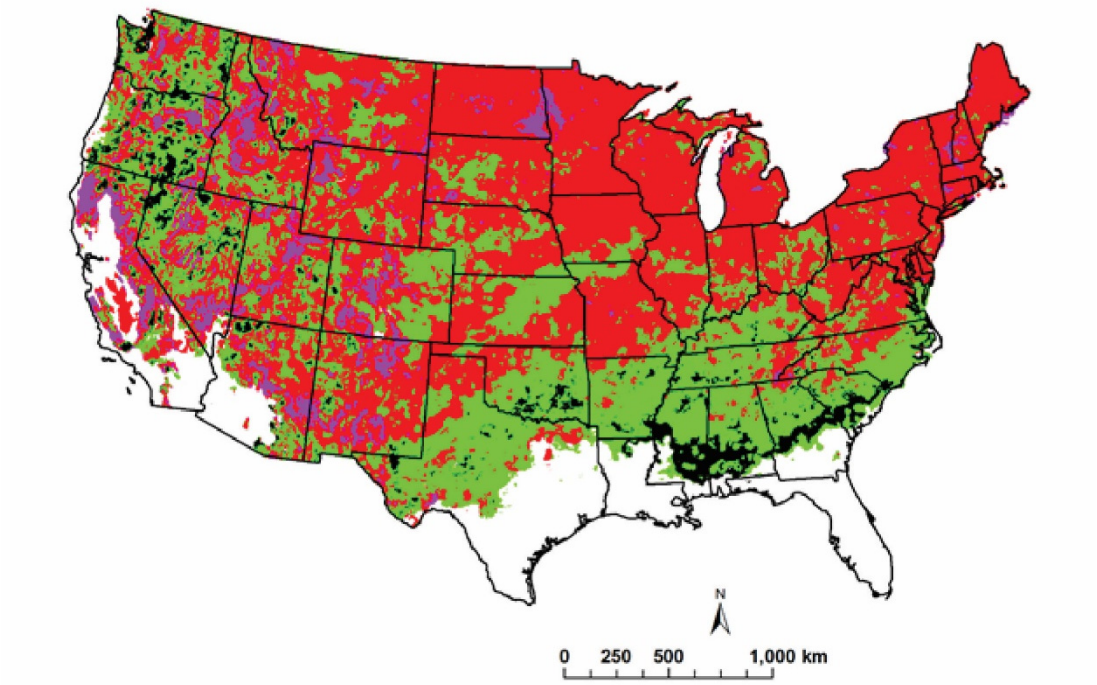

Figure 2. Trend of annual number of months with at least one month that had a day with a minimum temperature < 0°C over 25 years. Red denotes the significant ($p < 0.05$) decrease, green denotes the significant increase, purple denotes the non-significant decrease, black denotes the non-significant increase in minimum temperatures. Areas with no color denote not enough months with minimum temperature < 0°C for trend determination.

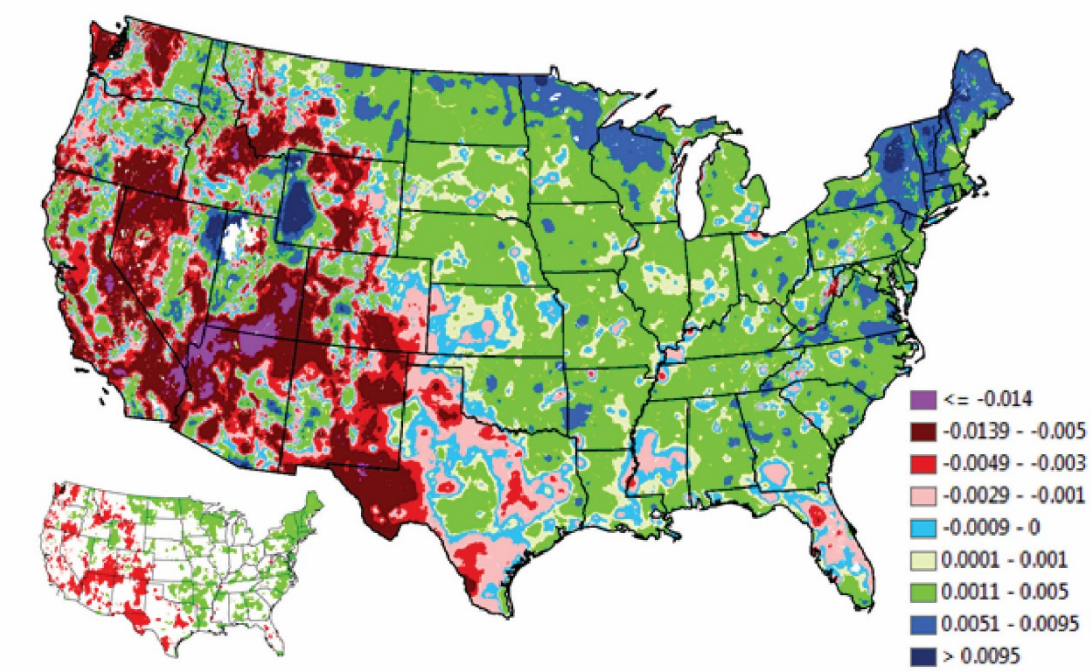

Figure 3. Pixels (1 km^2) with temporal trends in monthly dew point temperature (°C/month). The first and last legend classes represent the 1st and 99th percentiles. The insets maps are the probability of temporal trend, green indicates significant increase and red indicates a significant decrease.

concentrated in the west. The 1st and the 99th percentiles of the trend values for dew point temperatures were -0.014°C/month and +0.0095°C/month, respectively.

Monthly precipitation trends (Fig. 4) decreased significantly by 8.7% and were mostly concentrated along the Texas-Oklahoma-Louisiana border and scattered throughout the southern Appalachians (inset map in Fig. 4). The spatial distribution of precipitation trend values showed that the highest increases in precipitation were in the north and northeastern part of the nation (Fig. 4) with a rate (99th percentile) 0.072 mm/month and the lowest were in the southern part of the U.S. with a rate of (1st percentile) -0.1236 mm/month. Extreme values in increasing and decreasing precipitation were located in Washington, Oregon, and California. Decreasing precipitation occurred in Louisiana, Texas, Oklahoma, and southwestern North Carolina (1st percentile, Fig. 4). Increasing precipitation occurred in Maine and New York (99th percentile, Fig. 4). The overall changes in precipitation were only significant for small areas in the northeast (~3% significant increases, Nash et al. 2017) and in the south within Louisiana, Texas, and Oklahoma (~9% significant decreases, Nash et al. 2017) (see map inset in Fig. 4).

Due to the nearly continent-wide significant increase in monthly temporal trends of minimum temperature (Fig. 1B), PET monthly temporal trends also show a nearly continent-wide increase (Fig. 5). Most of the contiguous U.S. experienced an increase PET trend, with comparatively isolated clusters of significantly declining PET trends primarily in the Pacific Northwest and California (Fig. 5 inset). However, clusters of the highest increases in PET were also in the west. The 1st percentile in decreasing PET was -0.0156 mm/month and the 99th percentile in increasing PET was 0.0345 mm/month. Many of the changes in PET were significant increases ($p < 0.05$, inset map in Fig. 5) and small clusters of significant decreases were scattered in Washington, Oregon, California, and Florida.

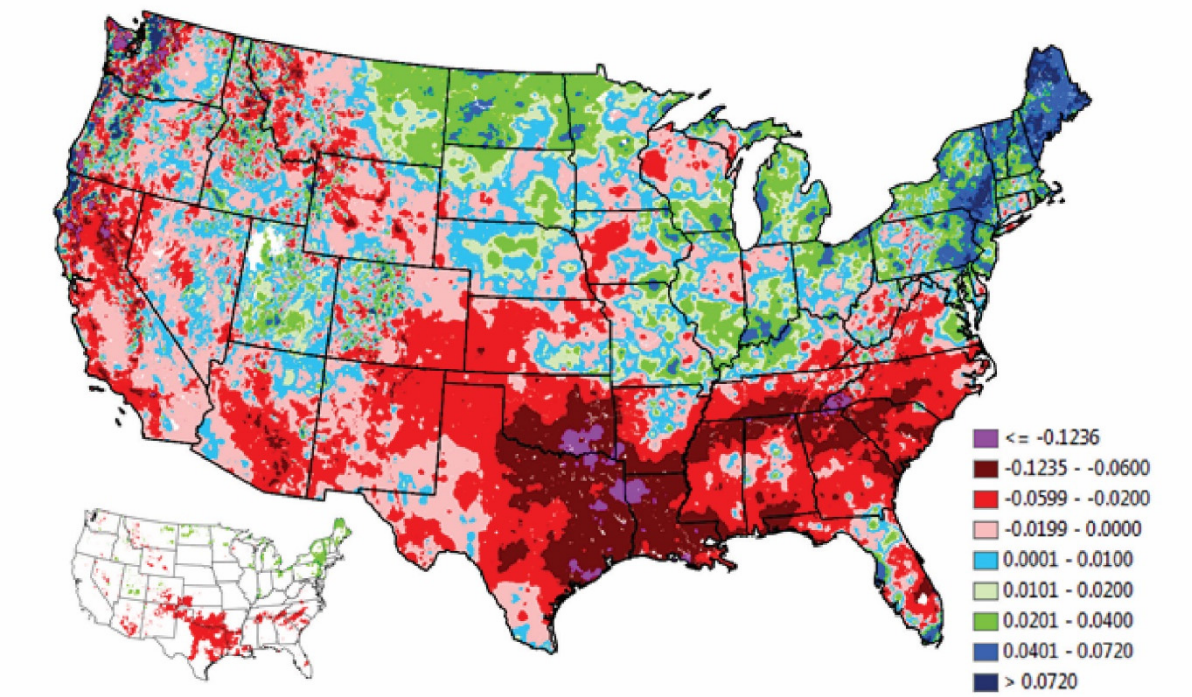

Figure 4. Pixels (1 km^2) with temporal trends in monthly precipitation (mm/month). The first and last legend classes represent the 1st and 99th percentiles. The insets maps are the probability of temporal trend, green indicates significant increase and red indicates a significant decrease.

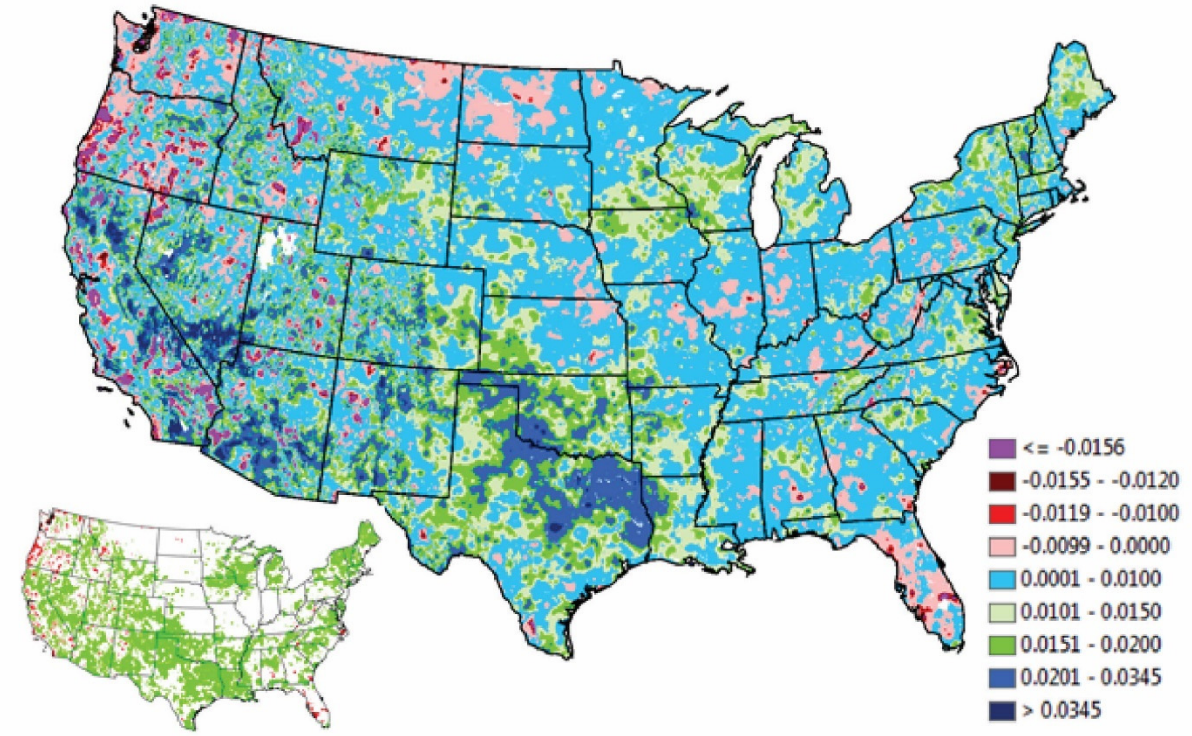

Figure 5. Pixels (1 km^2) with temporal trends in monthly PET (mm/month). The first and last legend classes represent the 1st and 99th percentiles. The inset map is the probability of temporal trend, green indicates significant increase and red indicates a significant decrease.

MI is a composite of precipitation, day length, average temperature and saturated vapor pressure [Equation 3] and represents the relative wetness (+ MI values) and dryness (- MI values) of an area. The spatial distribution of monthly MI trend values in Fig. 6A shows the magnitude and direction of change in monthly MI over the 25 years. While the positive increase in MI covered 31% of the U.S., only ~1% was a significant increase. Sixty-nine percent of the U.S. had an MI decrease with 14% having a significant decrease (inset map in Fig. 6A). North Dakota and Montana have the highest increase in MI, large areas in Louisiana and Texas have the lowest MI. The spatial distribution of the average MI in Fig. 6B presents the gradients in monthly average moisture conditions/regimes in the nation over the 25 years. The zero value of MI (purple polygons in Fig. 6B) where PET equals precipitation, stretches from eastern Texas to the northwestern U.S. and divides the nation into a relatively homogenous moist area to the east and drier areas to the west. The largest dry areas are in southern Arizona, California, and Nevada; and a mosaic of all MI groups in the northwest.

The spatial distribution of heat index (*AT*) (Fig. 7) shows the widespread of increase in *AT* values over 25 years. Seventy-eight percent of the U.S. experienced an increase in *AT* from 1989 to 2013; one-third of the total area experienced a significant increase in *AT* (inset map in Fig. 7). Most states experience high *AT*, except for North Dakota, and the coastal area in Washington and Oregon. Only ~3% of the USA had a significant decrease in *AT;* concentrated primarily in western Oregon and northern Montana (inset map in Fig. 7). The 1st and 99th percentile for *AT* were -0.0049 and 0.0088, respectively. Following Smoyer-Tomic and Rainham (2001), the spatial distribution of number of months for *AT* groups a-c (see Material and Method for group description) are presented in Figs 8A-C. Most areas had at least one month of *AT* values between 26.7 and 32.2°C (Fig. 6A; 26.7 $^{\circ}$C $\leq AT <$ 32.2°C). Values within top 20th percentile are mainly

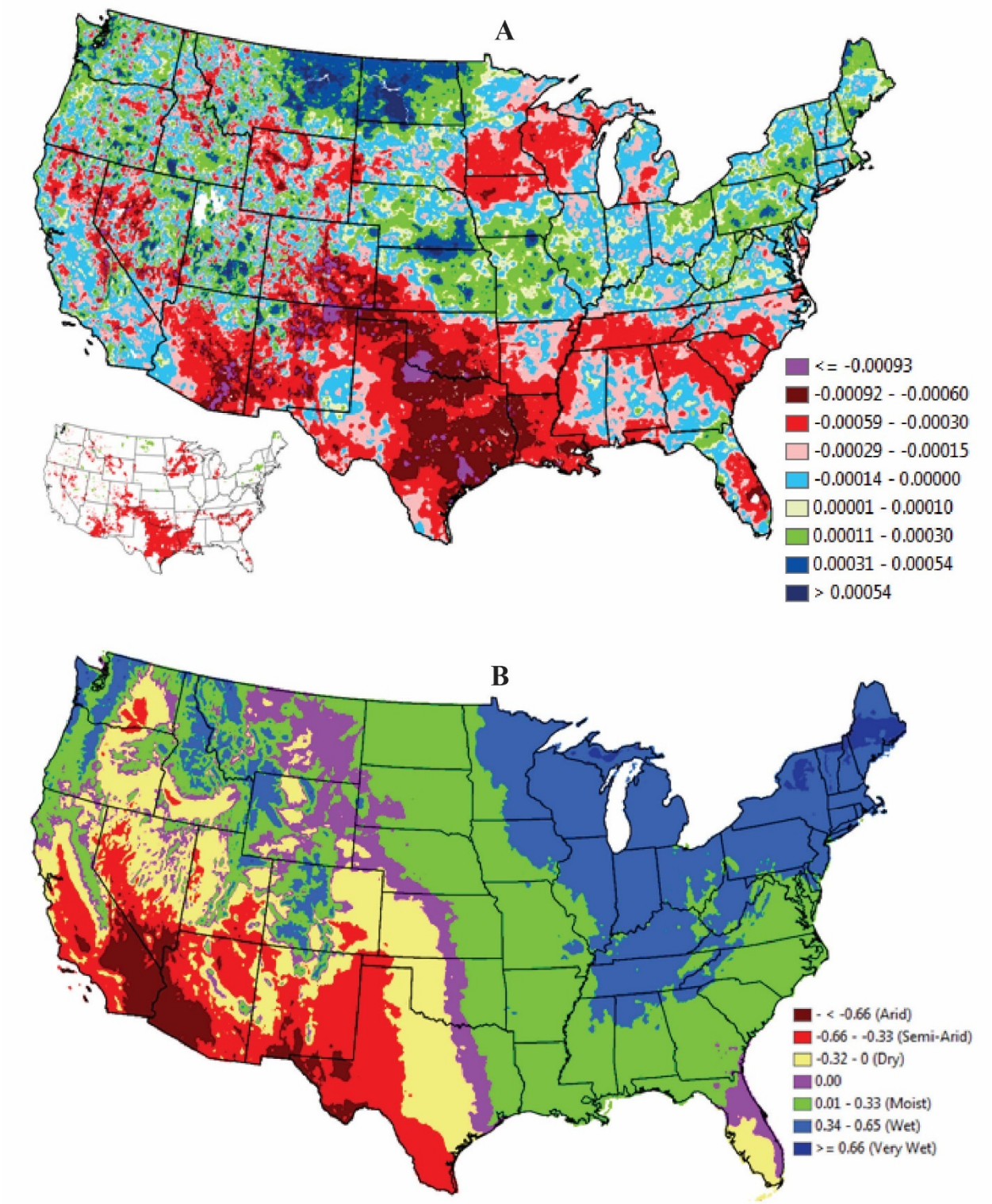

Figure 6. Pixels (1 km^2) with temporal trends in monthly (A) MI, the first and last legend classes represent the 1st and 99th percentiles. (B) Moisture regimes (Feddema (2005) categories) based on the average monthly moisture index (MI) over 25 years (1989-2013) a zero group is a divider between dry and wet areas. The inset map in (A) is the probability of temporal trend, green indicates significant increase and red indicates a significant decrease.

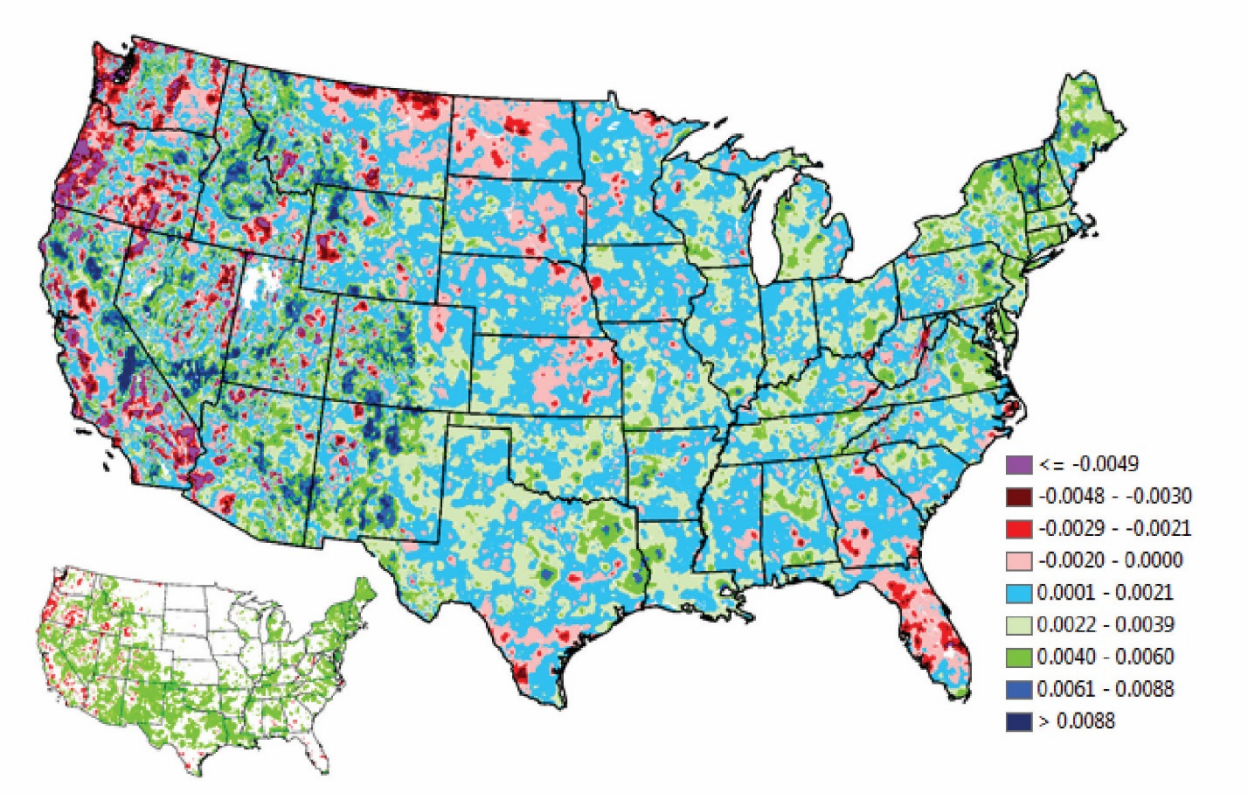

Figure 7. Pixels (1 km^2) with temporal trends in monthly *AT*. The first and last legend classes represent the 1st and 99th percentiles. The inset map is the probability of temporal trend, green indicates significant increase and red indicates a significant decrease.

concentrated in eastern states, Florida, and western states (Texas, New Mexico, Arizona, Nevada and California). *AT* values between 32.2˚C to 40.6˚C are clustered in a smaller geographic area (Fig. 8B). Areas in the top 10th percentile were concentrated in the southern coastal area extending from Florida to Texas. For *AT* between 40.6°C and 54.4°C, an even smaller area was covered, and the top 10th percentile areas were found mainly in southern Texas, Arizona, and California (Fig. 8C).

Average and variability are often used to describe climatic factors changes over time. We present the overall average and coefficient of variability (CV) of the monthly minimum, maximum, and average temperatures in Fig. 9. Highest average temperatures are clustered in the southern part of the U.S. and decreased toward the northern part of the U.S. mainly in North Dakota and Minnesota. While the average temperature decreases, highest variability occurs in northern

Midwestern states and in several clusters within the states of Utah, Idaho, and Montana. (Changes in temperatures using average and CV values based on different temporal scales are discussed below).

Annual: Average and Coefficient of Variability for Annual Precipitation, Potential Evapotranspiration (PET), and Moisture Index (MI).

The spatial distribution of average and CV for annual precipitation and annual PET are shown in Fig 10. Average precipitation was higher in the eastern and the north Pacific coastal areas than most of the western states (Fig. 10A). The general pattern of the precipitation was in longitudinal parallel bands at mid U.S. with clusters in the southern states (Alabama, Mississippi, and Louisiana) and western Washington and Oregon. Highest precipitation values are within these clusters. The variability (CV) in precipitation is the highest in areas with low precipitation: California, southern Nevada, and eastern Arizona on the southern border of New Mexico and Arizona. Variability radially decreases as one moves from the southwest toward the northeast.

PET ranged from 435 mm (~17 inches) in light blue areas in Fig. 10B (Northeast, areas around the Great Lakes, and in the high Rocky Mountains) to highest PET of at least 1000 mm (39 inches) in dark blue area (Florida, south Texas, south Arizona, southwest California and southern Nevada). This potential loss may or may not be compensated by the amount of precipitation. In order to consider the balance of PET with available precipitation, we combined the yearly precipitation and PET (Equation 3) to calculate the yearly MI. The annual average and CV of MI are shown in Fig. 11. The pattern of distribution for average annual MI (Fig. 11A) in the eastern part of U.S. was more dominated by precipitation (Fig. 10A & Fig. 10B) than PET (Fig. 10C & Fig. 10D). Highest variability in annual MI (Fig. 11B, in blue) extended in parallel bands from the north along the eastern border of the Dakotas to the eastern side of Texas.

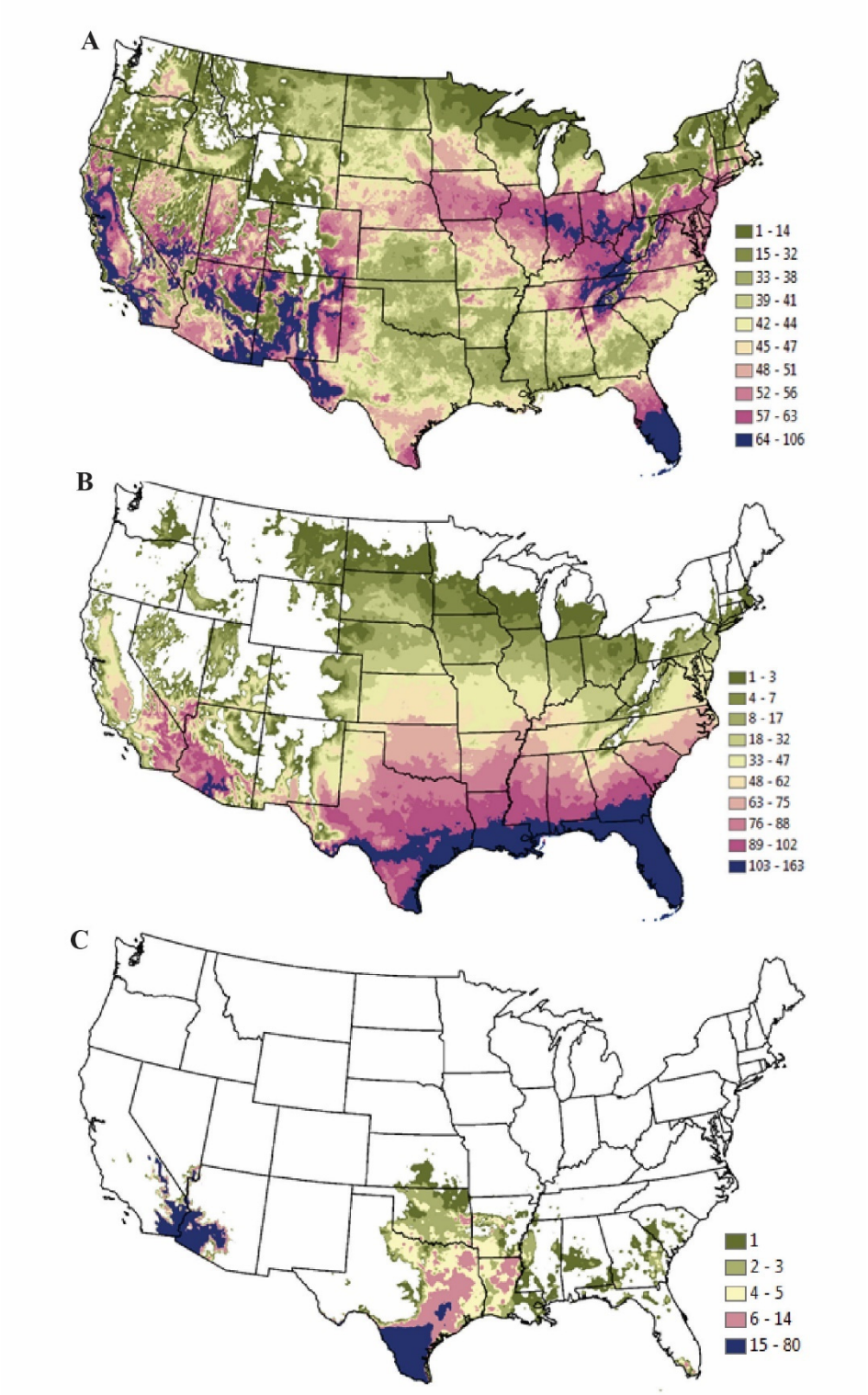

Figure 8. Distribution of total number of months (out of 300) that had at least one *AT* value in group: **A)** *fatigue possible with prolonged exposure and/or physical activity* (26.7°C ≤ *TA* ≤ 32.2°C) **B)** *sunstroke, heat cramp, and heat exhaustion possible with prolonged exposure and/or physical activity* (32.2°C < *TA* ≤ 40.6 °C) **C)** *sunstroke, heat cramp, or heat exhaustion likely, and heatstroke possible with prolonged exposure and/or physical activity* (40.6°C < *AT* ≤ 54.4°C).

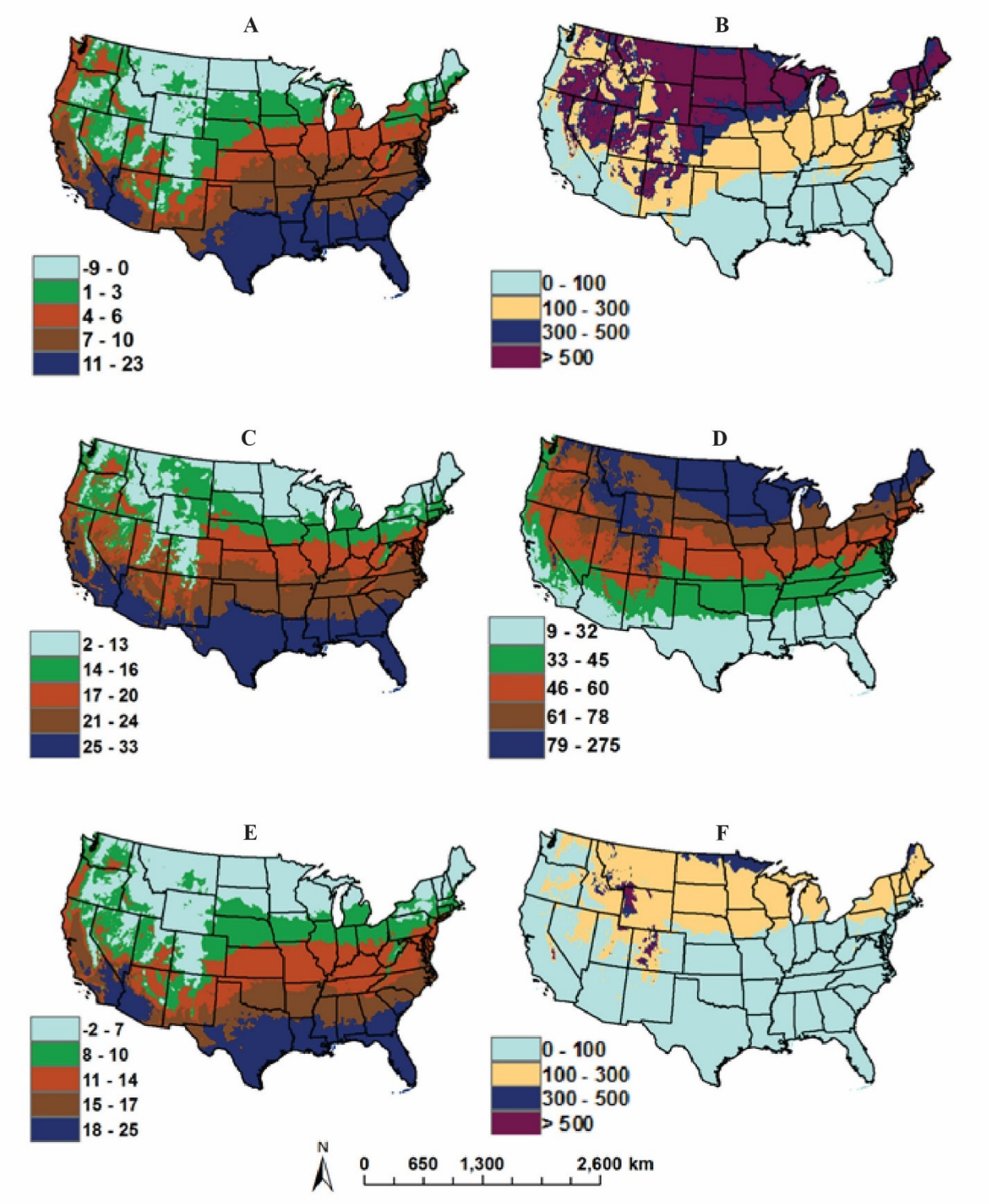

Figure 9. Average and coefficient of variability (CV) of monthly minimum temperature (A & B), monthly maximum temperature (C & D) and monthly average temperature (E & F) (n=300). The CV legend represents the absolute value (e.g. 100 is abs (±100)). Higher CV values represent higher variability in climatic factor.

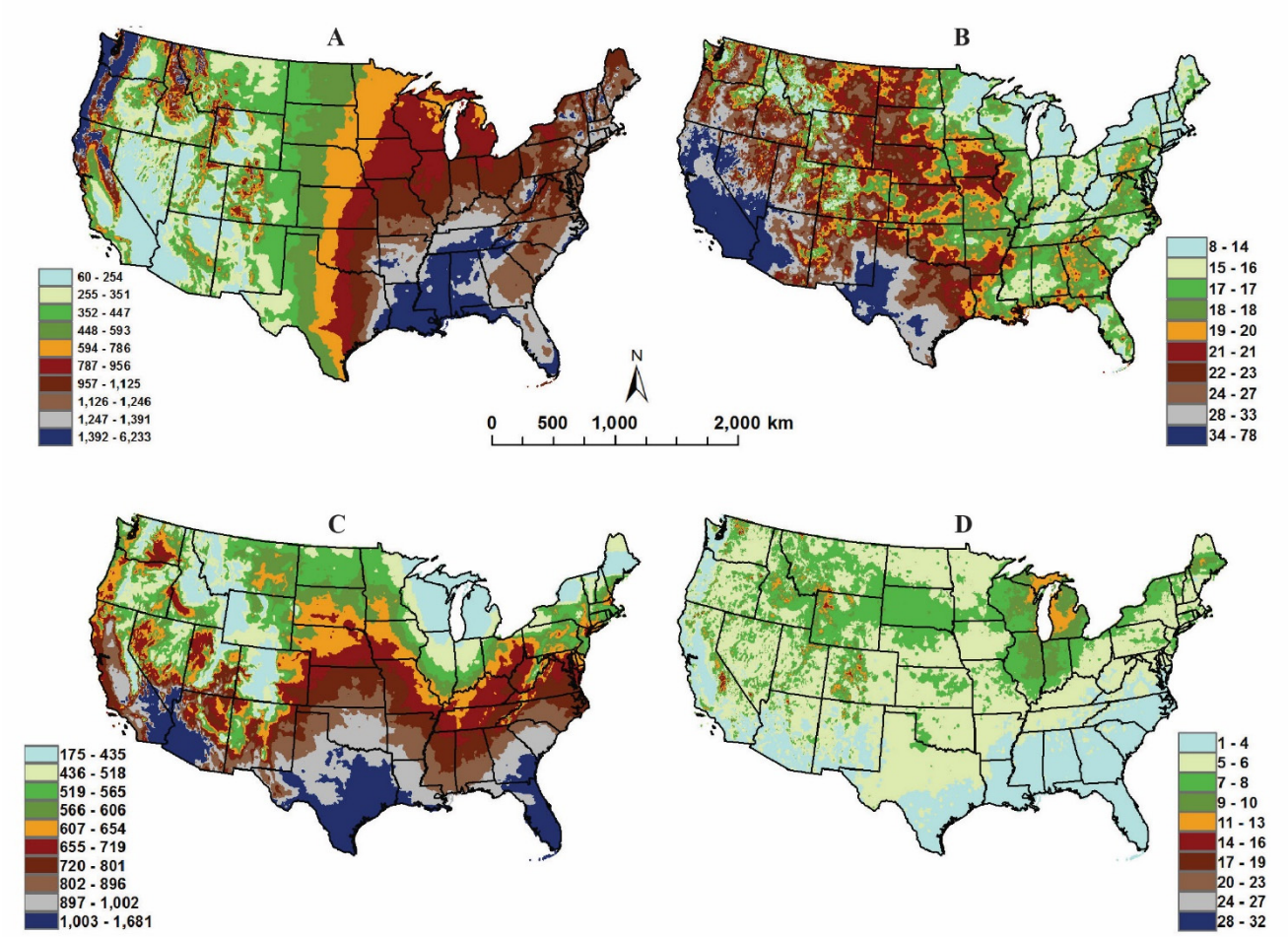

Figure 10. Precipitation annual average (A) and coefficient of variability (B), PET annual average (C) and coefficient of variability (D) (n=25).

Seasonal: Average and Coefficient of Variability for Seasonal Precipitation, Potential Evapotranspiration (PET), and Moisture Index (MI).

The spatial distribution pattern for precipitation varies with the temporal scales, which can be seen by comparing the average (Fig. 12) and CV (Fig. 13) for seasonal precipitation with that of the average of annual precipitation (Fig. 10A). The average amount of precipitation was higher in the winter season, followed by fall, spring, and summer (Table 1). The general spatial distribution of seasonal average precipitation (Fig. 12A-D) shows that higher precipitation was on the eastern side of the nation rather than that on the western side, except for the northern Pacific

coastal area which had low precipitation in summer only. The top 10th percentile of precipitation in the south-eastern states moves to southern coastal areas in summer (Fig. 12).

A significant increase in winter precipitation was mainly clustered in Michigan, Wisconsin, and Minnesota (Fig. 12A). For the spring season, a significant increase in precipitation -occurs in northern Minnesota, in most of North Dakota and northeastern Montana (inset maps in Fig. 12B). For summer and fall precipitation, smaller clusters with significant increases were within Maine and eastern New York (summer), mid-Montana and southern Nevada (fall). About 39% of the areas had significantly decreasing all season precipitation while increasing precipitation occurred in only 23% of the areas. Spring precipitation decreased more than in other season (13%) and it was mainly within Louisiana, Arizona and southern Nevada and California. The significant decrease in summer precipitation covered fewer areas than in the spring seasons (12%) (Fig. 12C). The significant decrease in fall precipitation (5%) was clustered mainly in South Carolina and Oklahoma (inset map in Fig. 12C). The overall monthly trend for precipitation showed that much of the significant decrease in precipitation was clustered in Oklahoma and Texas (Fig. 4).

Coefficient of variability (Fig. 13) describes the distribution of variability in precipitation at different temporal scales. In general, the variability of seasonal precipitation (Fig. 13) is greater in the western part of the nation than in the eastern part of the nation. Higher variability occurs in areas where the precipitation is low, at the center of the nation (Fig. 13) extending from north to south, reflecting the pattern in the distribution of average seasonal precipitation. Average seasonal precipitation (Fig. 12), closer to median value, is located at the center of the nation extending from north to south.

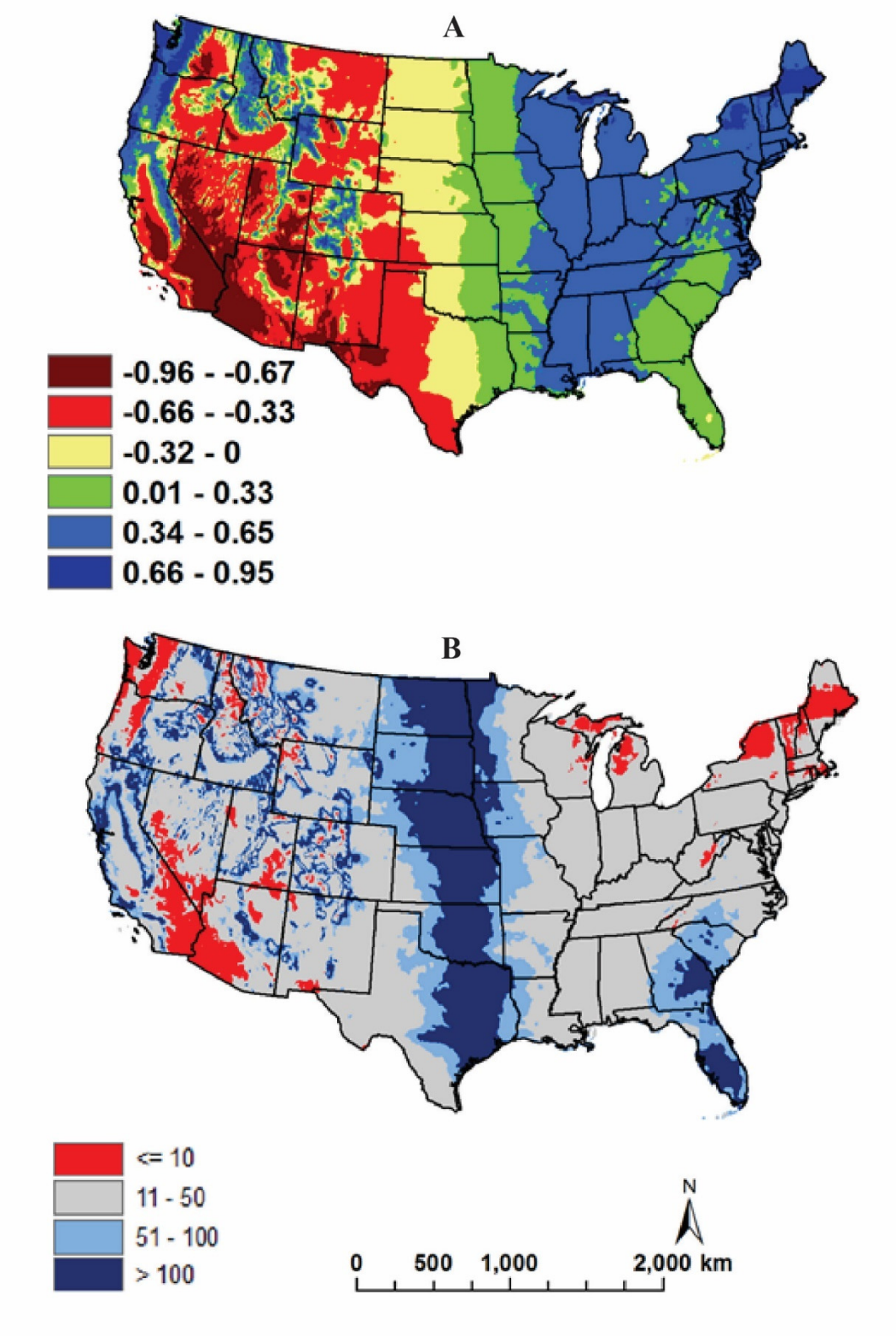

Figure 11. Yearly average for MI (A) and coefficient of variability (CV) (B) (n=25 years). The legend in (B) represents the absolute value of CV (e.g. <= 10 is <= abs (±10)).

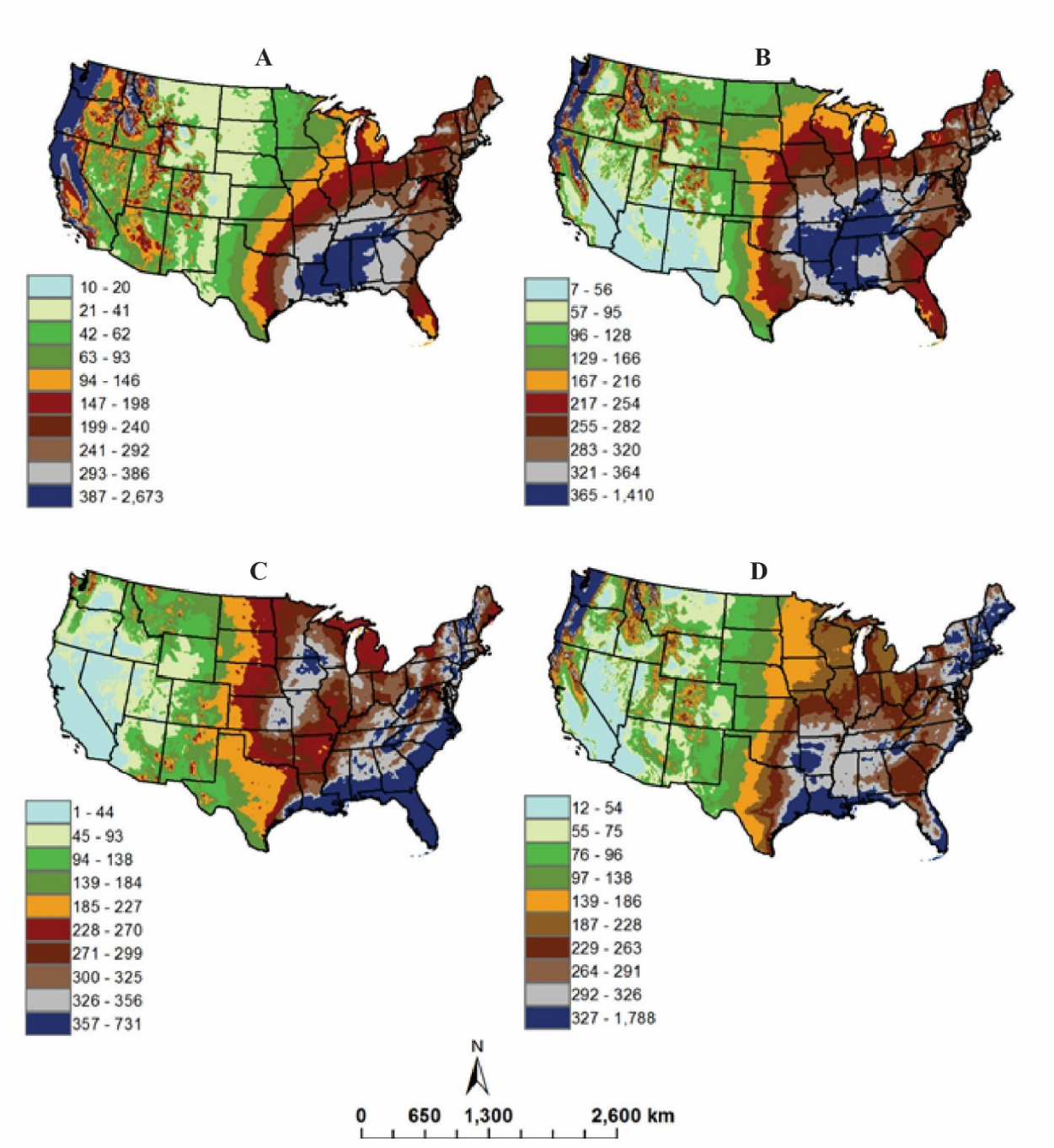

Figure 12. The ten quantiles for the average seasonal precipitation for (A) winter, (B) spring, (C) summer, and (D) fall.

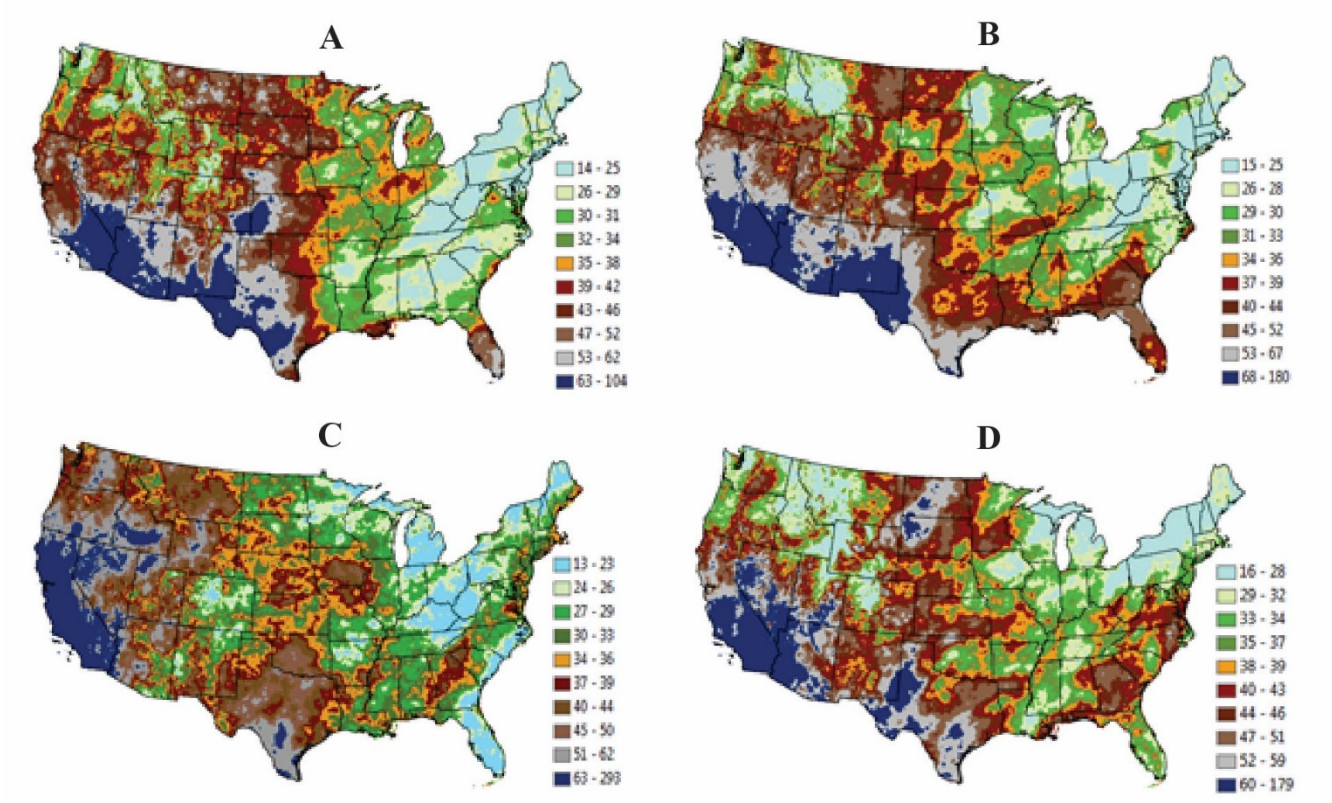

Figure 13. Coefficient of variability for (A) winter precipitation, (B) spring precipitation, (C) summer precipitation and (D) fall precipitation. Winter precipitation (Dec – Feb), spring precipitation (Mar – May), summer precipitation (Jun – Aug), fall precipitation (Sep – Nov).

Average seasonal value, seasonal trend and significant change in PET are presented in Figs 14 & 15. In all seasons, the highest PET annual average was located in the southern part of the nation, southern California, Nevada, Arizona, Texas, Alabama, Georgia, and Florida. While PET decreased in most areas in winter with less areal coverage in spring, PET increased significantly in approximately all areas in summer followed by fall (insets in Fig. 15). The spatial distribution of the average annual PET (Fig. 10C) was close in spatial distribution to that of the spring season (Fig. 14B).

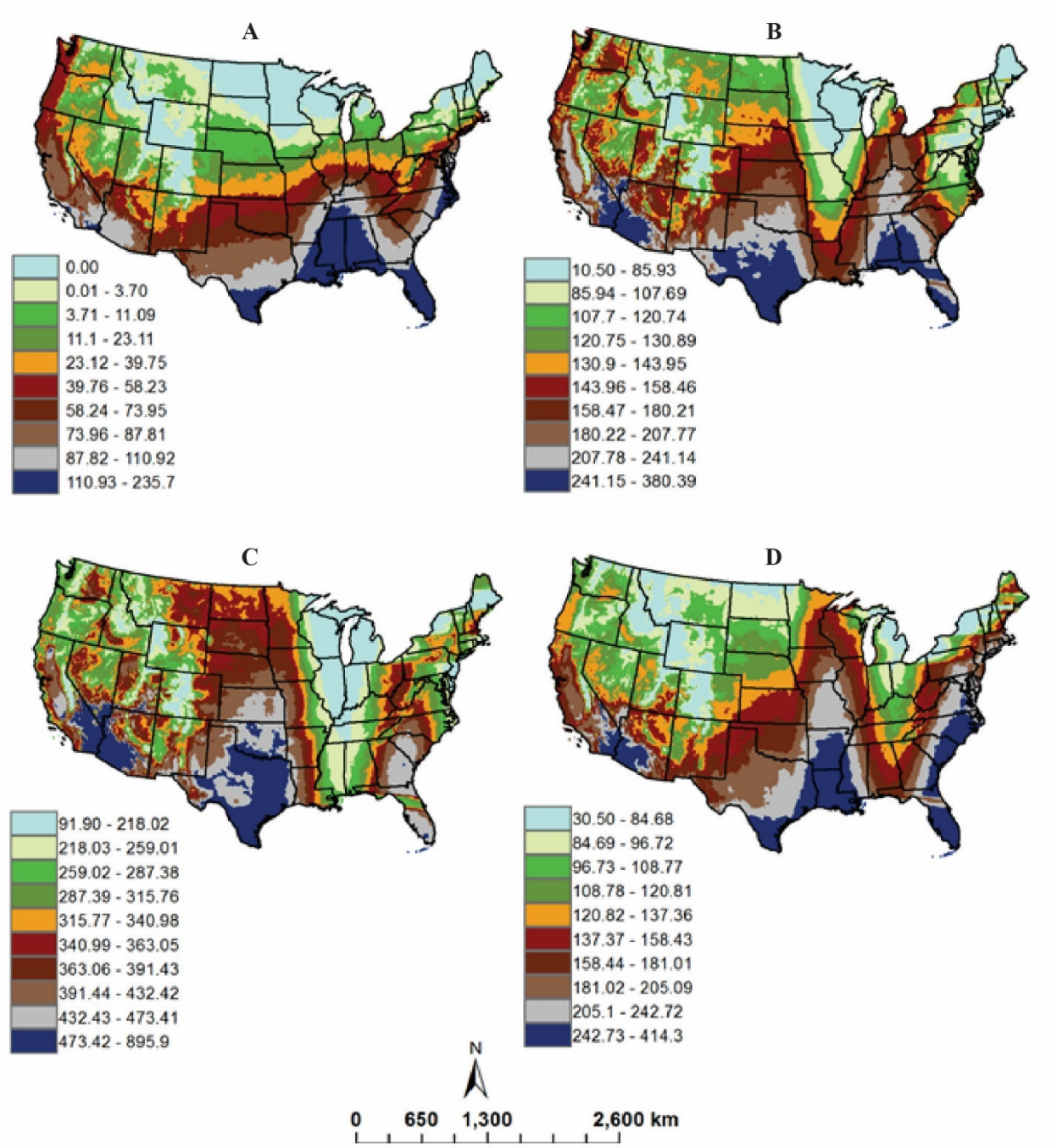

Figure 14. Average seasonal PET for (A) winter, (B) spring, (D) summer, and (E) fall. Winter precipitation (Dec – Feb), spring precipitation (Mar – May), summer precipitation (Jun – Aug), fall precipitation (Sep – Nov).

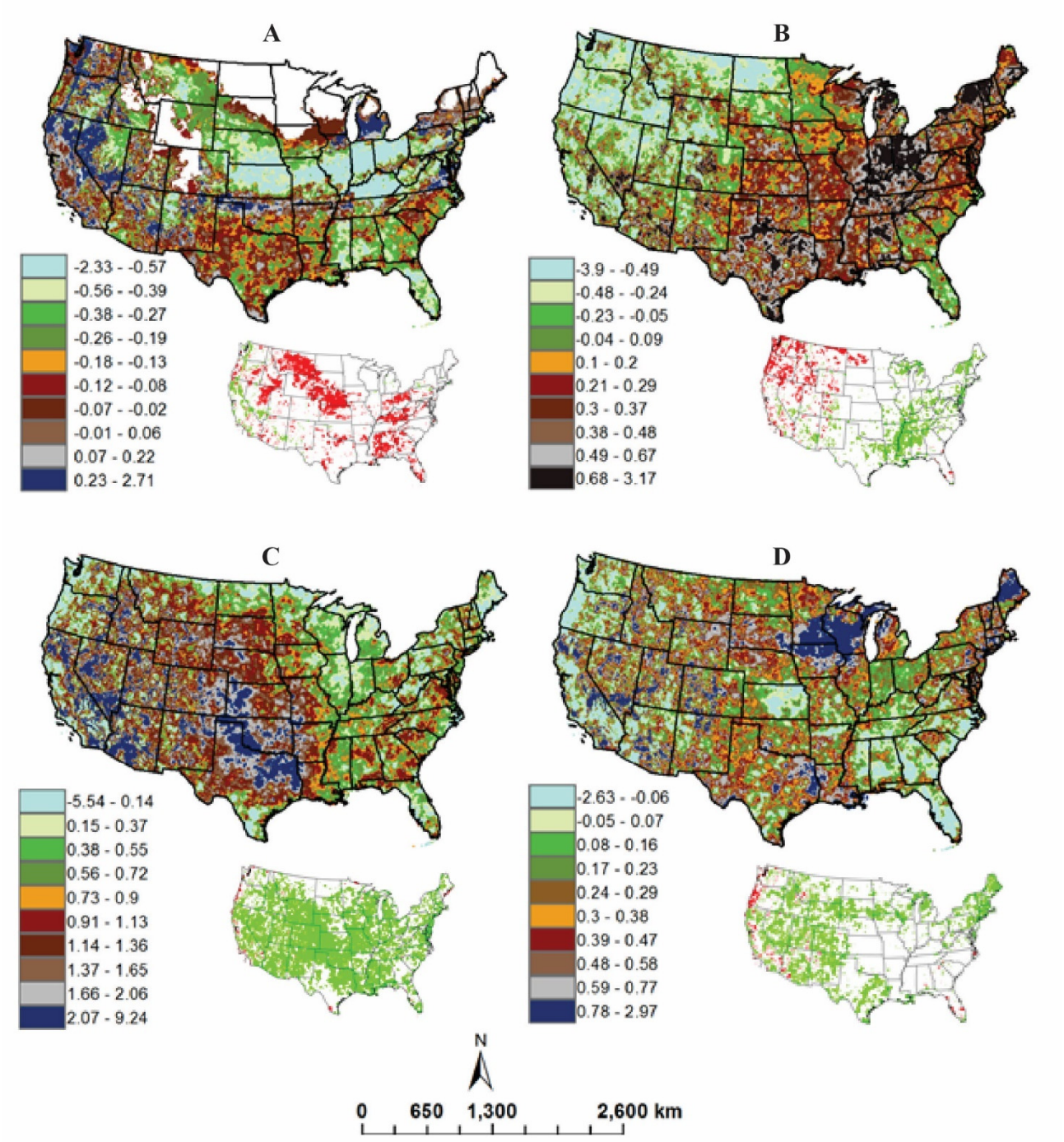

Figure 15. PET seasonal trend value for (A) winter, (B) spring, (C) summer and (D) fall. The inset figures are the probability of trend.

The distribution of the MI (Fig. 16), seasonally characterized by low MI values (drier) in the summer season, were spatially extended from mid-western to western U.S. Higher MI values (wetter) in winter extended from north to south (Fig. 16). Regardless of being seasonal or annual,

the eastern part of the nation was wetter than the west. The spatial distribution of the annual MI is more likely to be between fall/spring pattern, but it was much different than winter and summer seasons. MI increases significantly mostly in the northern part of the nation for winter and spring but decreases significantly in the southern/western parts (inset maps in Fig. 16).

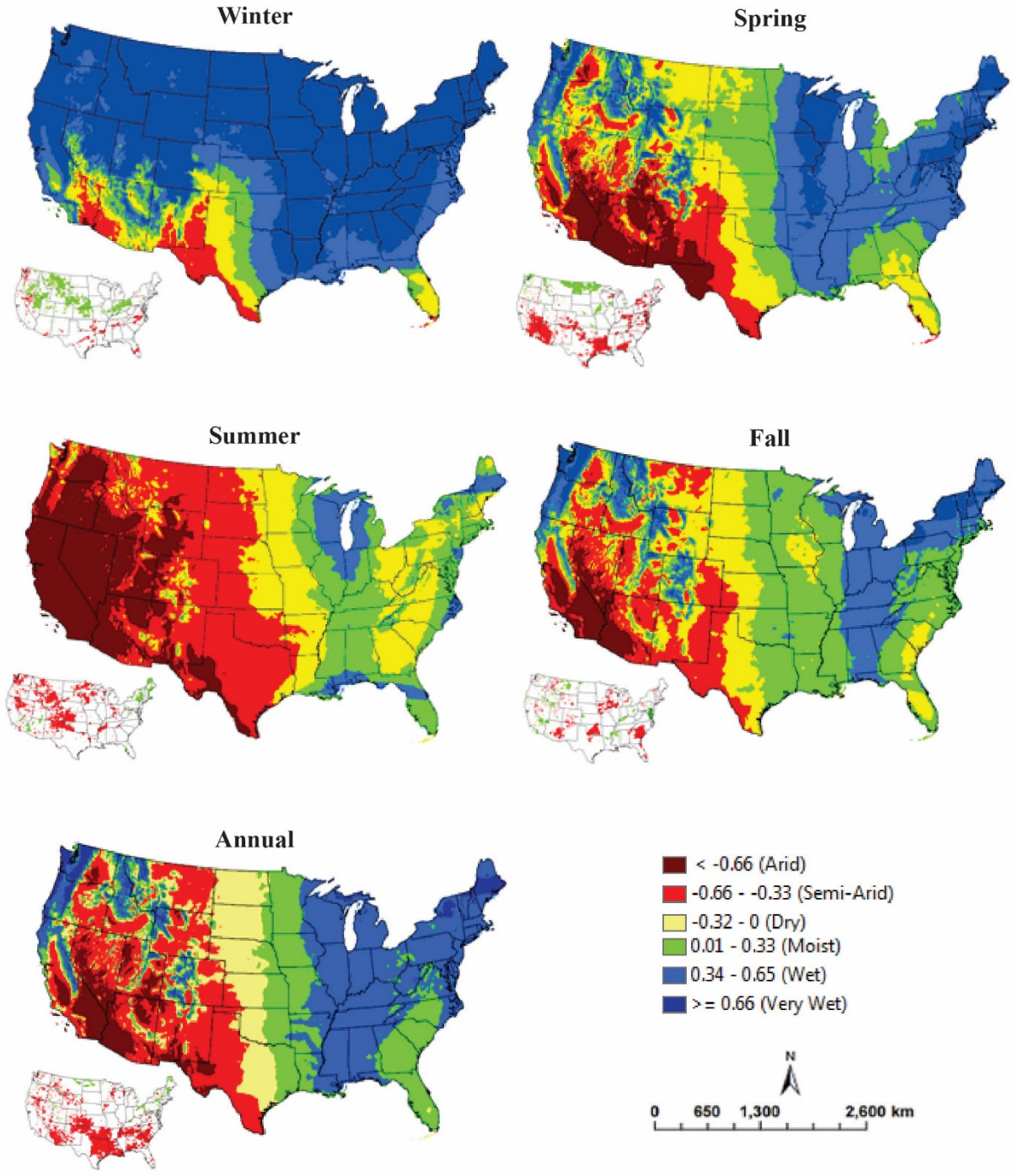

Figure 16. The 25-year average of MI for seasonal and annual. Legend is the Feddema et al. (2005) drought classification: very wet [MI ≥ 0.66], wet [0.66 > MI ≥ 0.33], moist [0.33 > MI ≥ 0.00], Dry [0.00 > MI ≥ -0.33], semi-arid [-0.33 > MI ≥ -0.66]; and arid [MI < -0.66]. Inset maps are the probability of trend, Red denotes significant decrease and green denotes significant increase.

Summary and Discussions

The general pattern of increase in temperature in the 48 contiguous states is consistent with other studies of climate change, where the trend for increasing average temperatures was higher for 1992-2008 than that of 1961-1979 (observational data, Karl and Melillo, 2009). An increasing trend in daily minimum temperatures (or nighttime temperature) was higher than the trend for daily maximum temperatures (daytime temperature) in western and central North America (Robeson, 2004). Millett et al. (2009) analyzed temperature and precipitation in the Central Plains of the U.S. in the 20th century and found increases in precipitation and minimum temperatures. The number of months per year that contain at least one month with a < 0°C temperature decreased significantly; Vincent and Mekis (2006) found a similar trend in Canada between 1950-2003. Although it is not within our study boundary, Alaska experienced the largest warming trend in temperature from 1951 to 2001 where the temperature increased from 0.8ºC to 1.9ºC, respectively. This warming occurred mostly in the winter season and coincided with the 1977 Arctic atmospheric and ocean regime shift (Hartmann and Wendler, 2005). Robles and Enquist (2011) found that precipitation in the United States increased over the past five decades by 5%; our findings suggest that < 3% of the U.S. had a significant increase in monthly precipitation during 1989−2013.

Dew-point is an essential element in fog formation. Hiatt et al. (2012) indicated that despite low rainfall, vegetation productivity did not decrease in the central and southern coastal regions in California due to fog deposition. Wet deposition of atmospheric nitrogen and sulfur via fog formations have been well documented (Fenn et al. 2000, 2003; Klemm and Wrzesinsky, 2007; Lovett and Tear, 2008; Polkowska et al. 2011). Spatial distribution of the dew point temperature changes can help inform fog formation locations.

Potential Evapotranspiration (PET) represents the amount of water loss via plant and soil transpiration. PET is estimated from temperature, water saturated vapor pressure (Equations 1 & 2) and daylight length which varies with season and spatial locations. Thus, it is important to look at precipitation and PET in concert to determine the magnitude and direction of water loss or gain across seasons and spatial location. Hinzman et al. (2005) reported that the difference between precipitation and PET decreased during the warm season from 1960 to 2000 in Alaska and was mainly related to an increasing in air temperature (precipitation did not change significantly). On the Tibetan Plateau where daytime temperature trend is unchanged, Shenbin et al. (2006) found that the negative trend in PET is more related to the regional monsoon circulation. Millett et al. (2009) in the Prairie Pothole Region of the U.S. found that an east to west moisture gradient steepened as temperature and precipitation shifted in the 20th century, resulting in a wetter eastern section and a drier western section. The Moisture index (MI) formally combines PET and precipitation, thus MI can demonstrate resulting effects of interactions of temperature and precipitation both across space and changes/shifts through seasons. Grundstein (2009) showed significant increases in annual MI (wetter conditions) for climate divisions in the Southeast and in a band across the north, stretching from South Dakota to New York. Areas that may not show annual shifts in MI may still have seasonal MI shifts which may be important due to hydrological, biological and biogeochemical dependence on the timing of available water. For example, decreases in snowfall or earlier snow melt in the Western U.S. impacts water storage, the timing of stream flows and the biota that rely on those streams (Hamlet et al. 2005; Mote et al. 2005). Likewise, an increase in precipitation in Great Yellowstone Ecosystem since 1977 has not been enough to compensate for water loss by PET. This deficit has been exacerbated by the increase in

minimum temperature which impacted snowpack and has resulted in a reduced flow through streams, especially in summer season (Chang and Hansen, 2014).

Conclusion

Our analysis per pixel for the entire U.S. offers a means of monitoring changes in trend direction and magnitude for a specific area of interest. Choosing the appropriate time scale (monthly, annual or seasonal) in climatic factors in building a relation with a response (e.g., vegetation, fills and spills from water bodies) is an important step to explore. The spatial and temporal analyses of these climatic factors combined with factors of interest (fires, health factors, environmental factors, etc.) can be used to examine different responses to direct impacts and/or climate changes in an area.

Implication

We envision the use of these data sets in diverse multidisciplinary studies and research. In previous studies, we used pixel-based univariate versus multivariate autoregression models with these climatic factors to demonstrate that long-term monitoring can potentially detect broad-scale, slow changes, such as those caused by climate change over decades, as well as more local and rapid changes such as those caused by fire, agriculture, land clearing, and habitat restoration over time. (Nash et al. 2014, 2017). Such monitoring can provide environmental decision-makers with early warning signals for widespread general trends, as well as a means to identify specific areas where land conditions are degrading or improving. Using a similar multivariate approach, we assessed the dynamic interaction between climate, argan trees, local communities, rural household welfare, and forest conservation and sustainability in Morocco (Lybbert et al. 2011). We have applied Thornthwaite and Mather's (1957) approach using the monthly PET, precipitation, and depth of soil to calculate water balance in selected forested areas in U.S. (Nash unpublished data). The distribution of significant changes, extremes, variability and averages at different temporal scales provide a road map to the availability and important trends of temperature, rainfall and available moisture that have been occurring across the U.S.

References

Chang, T. and A.J. Hansen, 2014. Climate Change Brief: Greater Yellowstone Ecosystem. Landscape. *Climate Change Vulnerability Project*. p. 1-8. http://www.montana.edu/lccvp/documents/LCCVP_GYE_ClimateBrief.pdf. Accessed Dec 7, 2017.

Enquist, C.A.F., E.H. Girvetz, and D.F. Gori, 2008. A climate change vulnerability assessment for biodiversity in New Mexico, Part II: Conservation implications of emerging moisture stress due to recent climate changes in New Mexico. *The Nature Conservancy*.

Feddema, J.J., 2005. A revised Thornthwaite-type global climate classification. *Physical Geography*, 26(6): 442-466.

Fenn, M.E., M.A. Poth, S.L., Schilling, and D.B. Grainger, 2000. Throughfall and fog deposition of nitrogen and sulfur at an N-limited and N-saturated site in the San Bernardino Mountains, southern California. *Canadian Journal of Forest Research,* 30:1476-1488.

Fenn, M.E., R. Haeuber, G.S. Tonnesen, J.S. Baron, S. Grossman-Clarke, D. Hope, D. A. Jaffe, S. Copeland, L. Geiser, H.M. Rueth, and J.O. Sickman, 2003. Nitrogen Emissions, Deposition, and Monitoring in the Western United States. *BioScience,* 53(4): 391-403.

Forsythe, W.C., E.J. Rykiel Jr., R.S. Stahl, H.Wu, and R.M. Schoolfield, 1995. A model comparison for daylength as a function of latitude and day of the year. *Ecological Modeling* 80:87-95.

Grundstein, A., 2009. Evaluation of climate change over the continental United State using a moisture index. *Climate Change*, 93:103-115. DOI 10.1007/s10584-008-9480-3.

Hamlet, A.F., P.W. Mote, M.P. Clark, and D.P. Lettenmaier, 2005. Effects of temperature and precipitation variability on snowpack trends in the western United States. *Journal of Climate*, *18*(21), 4545-4561.

Hartmann, B., and G., Wendler, 2005. The Significance of the 1976 Pacific Climate Shift in the Climatology of Alaska. Journal of Climate, 18: 4824-4839.

Hamon, W.R., 1961. Estimating potential evapotranspiration. *Journal of the Hydraulics Division, American Society of Civil Engineers* 87:107-120.

Hiatt, C., D. Fernandez, and C. Potter, 2012. Measurements of fog water deposition on the California central coast. *Atmospheric and Climate Science* 2: 525-531.

Hinzman, L.D., N.D. Bettez, W.R. Bolton, et al. 2005. Evidence and implications of recent climate change in northern Alaska and other Arctic Regions, *Climatic Change*, 72: 251–298. DOI: 10.1007/s10584-005-5352-2.

Karl, T. R., J. T. Melillo, and T. C. Peterson, 2009: Global Climate Change Impacts in the United States. T.R. Karl, J.T. Melillo, and T.C. Peterson, Eds. Cambridge University Press, 189 pp. Online at: http://downloads.globalchange.gov/usimpacts/pdfs/climate-impacts-report.pdf

Klemm, O., and T. Wrzesinsky, 2007. Fog deposition fluxes of water and ions to a mountainous site in Central Europe. *Tellus*, 59: 705-714.

Lovett, G.M., and T.H. Tear, 2008. Threats from Above: Air Pollution Impacts on Ecosystems and Biological Diversity in the Eastern United States. The Nature Conservancy and the Cary Institute of Ecosystem Studies.

Lybbert, T.J., A. Aboudrare, D.J. Chaloud, N. Magnan, and M.S. Nash, 2011**.** Booming Markets for Moroccan argan oil appear to benefit some rural households while threatening the endemic argan forest. *Proceeding of the National Academy of Science 108:13963-13968.*

Millett, B.V., W.C. Johnson, and G.R. Guntenspergen, 2009. Climate trends of the North American prairie pothole region 1906–2000. Climatic Change, 93: 243–267.

Mote, P.W., A.F. Hamlet, M.P. Clark, and D.P. Lettenmaier, 2005: Declining mountain snowpack in western North America. Bull. Amer. Meteor. Soc., 86, 39–49.

Nash, M.S., D.F. Bradford, J.D. Wickham, and T.G. Wade, 2014. Detecting change in landscape greenness over large areas: An example for New Mexico, USA. *Remote Sensing of Environment*. 150: 152-162.

Nash, M.S., J. Wickham, J. Christensen, and T. Wade, 2017. Changes in landscape greenness and climatic factors over 25 years (1989-2013) in the USA. *MDBI Remote Sensing*, 9 (3), 295; doi:10.3390/re9030295.

Perry, A.G., M.J. Korenberg, G.G. Hall, and K.M. Moore, 2011. Modeling and syndromic surveillance for estimating weather-induced heat-related illness. *Journal of Environment and Public Health*, 1-10, doi: 10.1155/2011/750236.

Polkowska, Ż., T. Górecki, and J. Namieśnik, 2011. Determination of atmospheric pollutants in wet deposition. *Environmental Reviews*, 19: 185-213, https://doi.org/10.1139/a11-006

Robeson, S.M., 2004. Trends in time-varying percentiles of daily minimum and maximum temperature over North America. *Geophysical Research Letters*, 31, DOI: 1029/2003GL019019.

Robles, M.D., and C. Enquist, 2011. Managing changing landscapes in the Southwestern United States. *The Nature Conservancy*. Tucson, Arizona. 26 pp. Monitoring Systems Laboratory, Office of Research and Development, U.S. Environmental Protection Agency, Cincinnati, Ohio.

Shenbin, C., L. Yunfeng L., and A. Thomas, 2006. Climatic change on the Tibetan plateau: potential evapotranspiration trends from 1961–2000. *Climatic Change,* 76: 291–319. DOI: 10.1007/s10584-006-9080-z

Smoyer-Tomic, K.E., and D.G.C. Rainham, 2001. Beating the heat: development and evaluation of a Canadian hot weather health-response plan. *Environmental Health Perspectives*. 109(12) 1241-1248.

Thorne, J., R. Boynton, L. Flint, A. Flint, and T. Le, 2012. Development and Application of Downscaled Hydroclimatic Predictor Variables for Use in Climate Vulnerability and Assessment Studies. *California Energy Commission*. Publication number: CEC-500-2012-010.

Thornthwaite, C.W., J.R. Mather, and D.B. Carter, 1957. Instruction and tables for computing potential evapotranspiration and the water balance. *Drexel Institute of Technology, Philadelphia. Publications in climatology*, 10(3):185-311.

Vincent, L. and E. Mekis, 2006. Changes in daily and extreme temperature and precipitation indices for Canada over the twentieth century. *Atmosphere-Ocean, 44*, 177−193.

Willmott, C.J. and J.J. Feddema, 1992. A More Rational Climatic Moisture Index. *The Professional Geographer*, 44(1), 84-88.

United States
Environmental Protection
Agency

Office of Research
and Development (8101R)
Washington, DC 20460

Official Business
Penalty for Private Use
$300

EPA/600/S-17/434
October 2017
www.epa.gov

Please make all necessary changes on the below label, detach or copy, and return to the address in the upper left-hand corner.

If you do not wish to receive these reports CHECK HERE ☐; detach, or copy this cover, and return to the address in the upper left-hand corner.

PRESORTED STANDARD
POSTAGE & FEES PAID
EPA PERMIT No. G-35